A Journal of the Gesellschaft Deutscher Chemiker

Angewandte International Edition GDCh Chemie

www.angewandte.org

## Accepted Article

**Title:** ACQ-to-AIE Transformation: Tuning Molecular Packing by Regioisomerization for Two-photon NIR Bioimaging

**Authors:** Yuanyuan Li, Shunjie Liu, Huwei Ni, Haoke Zhang, Hequn Zhang, Clarence Chuah, Chao Ma, Kam Sing Wong, Jacky W. Y. Lam, Ryan T. K. Kwok, Jun Qian, Xuefeng Lu, and Ben Zhong Tang



**To be cited as:** *Angew. Chem. Int. Ed.* 10.1002/anie.202005785

**Link to VoR:** https://doi.org/10.1002/anie.202005785

WILEY-VCH

10.1002/anie.202005785

WILEY-VCH

COMMUNICATION

# ACQ-to-AIE Transformation: Tuning Molecular Packing by Regioisomerization for Two-photon NIR Bioimaging

Yuanyuan Li[+], Shunjie Liu[+], Huwei Ni[+], Haoke Zhang, Hequn Zhang, Clarence Chuah, Chao Ma, Kam Sing Wong, Jacky W. Y. Lam, Ryan T. K. Kwok, Jun Qian*, Xuefeng Lu*, Ben Zhong Tang*

[*] Dr. Y. Li, Dr. S. Liu, Dr. H. Zhang, Mr. C. Chuah, Prof. J. W. Y. Lam, Prof. R. T. K. Kwok, Prof. B. Z. Tang*
Department of Chemistry, Hong Kong Branch of Chinese National Engineering Research Center for Tissue Restoration and Reconstruction, Institute for Advanced Study, Department of Chemical and Biological Engineering, State Key Laboratory of Molecular Neuroscience and Division of Life Science
The Hong Kong University of Science and Technology
Clear Water Bay, Kowloon, Hong Kong, China
E-mail: tangbenz@ust.hk

Prof. X. Lu*
Department of Materials Science
Fudan University
Shanghai 200438, China
E-mail: luxf@fudan.edu.cn

Mr. H. Ni, Dr. H. Zhang, Prof. J. Qian*
State Key Laboratory of Modern Optical Instrumentations, Centre for Optical and Electromagnetic Research, College of Optical Science and Engineering
Zhejiang University
Hangzhou 310058, China
E-mail: qianjun@zju.edu.cn

Dr. H. Zhang
Interdisciplinary Institute of Neuroscience and Technology (ZIINT), the Second Affiliated Hospital, School of Medicine, Zhejiang University Hangzhou, 310020, China

Mr. C. Ma, Prof. K. S. Wong
Department of Physics
The Hong Kong University of Science and Technology
Clear Water Bay, Kowloon, Hong Kong, China

Prof. B. Z. Tang*
Center for Aggregation-Induced Emission, SCUT-HKUST Joint Research Institute, State Key Laboratory of Luminescent Materials and Devices
South China University of Technology, Guangzhou 510640, China
HKUST-Shenzhen Research Institute No. 9 Yuexing 1st RD, South Area, Hi-tech Park, Nanshan, Shenzhen, 518057, China
[+] These authors contributed equally to this work.

Supporting information for this article is given via a link at the end of the document.

**Abstract:** The traditional molecule's strategic designs for highly bright solid-state luminescent materials rely on weakening the intermolecular π-π interactions, which may limit diversity when developing new materials. Herein, we propose a strategy of tuning molecular packing mode by regioisomerization to regulate the solid-state fluorescence. TBP-*e*-TPA with a molecular rotor in the *end* position of planar core adopts a long-range cofacial packing mode, of which in the solid state is almost non-emissive. By shifting molecular rotors to the *bay* position, the resultant TBP-*b*-TPA possesses a discrete cross packing mode, giving a quantum yield of 15.6 % ± 0.2%. These results demonstrate the solid-state fluorescence efficiency's relationship with the molecule's packing mode. Thanks to the good photophysical properties, TBP-*b*-TPA nanoparticles exhibit excellent two-photon deep brain imaging. This molecular design philosophy provides a new way of designing highly bright solid-state fluorophores.

Solid-state luminescent materials have revealed exceptional abilities for practical applications in various fields such as optoelectronic devices, chemical sensing and bio-imaging owing to their outstanding photoluminescence quantum yields (PLQYs), and excellent photostability.[1] Whereas, most conventional luminophores often emit strongly as isolated molecules while showing negligible emission when aggregated or in the solid state, with the strong intermolecular π-π interaction inducing aggregation-caused quenching (ACQ) effect.[2] To address this issue, Tang et al. in 2001 introduced a new aggregation-induced emission (AIE) concept.[3] AIE luminogens (AIEgens) adopt twisted structures showing outstanding solid-state photoluminescence (PL) property via restricting the intermolecular π-π interactions.[4] Although AIE has now gained extensive attention as cutting-edge technology for a wide variety of applications, the molecular design philosophy for new AIEgens is still scarce.

To date, AIEgens are usually designed by the guideline of "backbone twisting + molecular rotor" with a mechanism of restriction of intramolecular motion (RIM).[5] Given the excellent optical properties and rich in a variety of ACQ molecules, transforming them into AIE-active provides an alternative way to design highly bright dyes.[6] Generally, ACQ-to-AIE transformation can be realized by incorporating twisted AIEgens, propeller molecules or bulky substituents into planar ACQ molecules to

10.1002/anie.202005785




prevent close cofacial packing.[7] However, this strategy does not apply to ACQ fluorophores with an extensive π-conjugated system, such as perylene bisimides.[8] We reason that besides efforts on restricting the tight cofacial packing among the molecules, controlling molecular packing is a fundamental issue for achieving optimized solid-state fluorescence efficiency. Tang *et al.* attested a significant impact of structural (*Z*)-/(*E*) isomerization on molecular packing.[9] The (*Z*) isomer formed regular particles with a green emission, while the (*E*) counterpart giving a cable-like structure (blue-emissive). Recently, Liu *et al.* attached an AIE moiety to a chiral glutamic acid.[10] The resulting molecule exhibited a solvent-driven molecular packing, giving a morphology-related chirality transfer. Prasad *et al.* regulated the structure of isomers to realize ACQ-to-AIE transformation, owing to the absence of interplay between the excited states.[11] These insightful strategies inspire new ideas for regulating solid-state fluorescence property. However, the molecular packing mode remains vague, posing a challenge for further understanding the solid-state fluorescence property. On the other hand, single crystal analysis of fluorophores with different architecture provides a strong support for exploring the relationship between fluorescence efficiency and packing mode.[12] Whereas, only rough conclusions such as "preventing the intramolecular π-π stacking in crystals enables high solid-state fluorescence QY", can be obtained. The shortage of precise guidelines for tuning of molecular packing hinders the further development of new solid-state fluorescence materials.

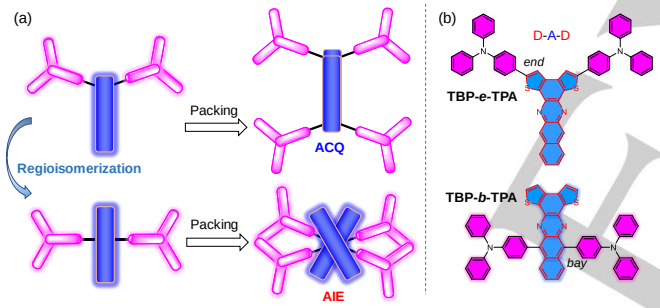


**Figure 1.** (a) Schematic illustration of tuning molecular packing by regioisomerization. (b) Chemical structures of TBP-*e*-TPA and TBP-*b*-TPA.

Herein, we proposed a precise strategy of tuning molecular packing by regioisomerization to regulate the solid-state fluorescence. As shown in Figure 1a, conventional dyes with large planar π-conjugated structure generally suffer from strong π-π interactions. Even end-capped with twisted molecular rotors, tight molecular packing can still exist in a tail-to-tail mode, resulting in no or weak emission in the solid/aggregate state (ACQ). If we shift the molecular rotor from *end* to the *bay* position (middle), the resultant steric hindrance may change the molecular packing mode without altering the π-conjugated core, which is possible for improving the solid-state fluorescence. Proof-of-concept, TBP-*b*-TPA with a molecular rotor in *bay* position shows a typical AIE characteristic with a NIR emission (687 nm) and a high solid-state QY of 15.6 % ± 0.2%, while its regioisomer TBP-*e*-TPA with the *end*-decorated molecular rotor is almost non-emissive (QY = 0.2% ± 0.1%). Molecular packing was revealed by single-crystal X-ray diffraction analysis to play an essential part in determining the efficiency of solid-state fluorescence. The ACQ-dominated TBP-*e*-TPA adopts a long-range cofacial packing mode, while the AIE-active TBP-*b*-TPA shows a discrete cross packing mode. Finally, given the high π-conjugation and donor-acceptor based structure, TBP-*b*-TPA nanoparticles were applied for two-photon deep brain imaging with high clarity. The present strategy of tuning molecular packing mode to regulate the solid-state fluorescence will inspire new ideas for exploring highly bright dyes.

The synthetic routes and characterization of TBP-*e*-TPA and TBP-*b*-TPA associated with intermediates are given in the Supporting Information (Figure 1b, Scheme S1, Figure S1-S6). Dithieno[2,3-a:3',2'-c]benzo[i]phenazine (TBP) with a large π-conjugated planar structure was designed and synthesized, which could not only act as acceptor unit allowing a great electron delocalization but also provide a platform for intermolecular interactions. To tune the molecular packing, twisted molecular rotor triphenylamine (TPA) grafted to a position at the *end* of TBP core is defined as TBP-*e*-TPA. While, TBP-*b*-TPA is denoted as the molecule with TPA in the *bay* of central TBP core. Due to the steric effect at the *end*, TBP-*e*-TPA may choose to pack in a tail-to-tail way (Figure 1a). The resultant intermolecular π-π interaction may result in fluorescence quenching in the solid/aggregate state.[2]

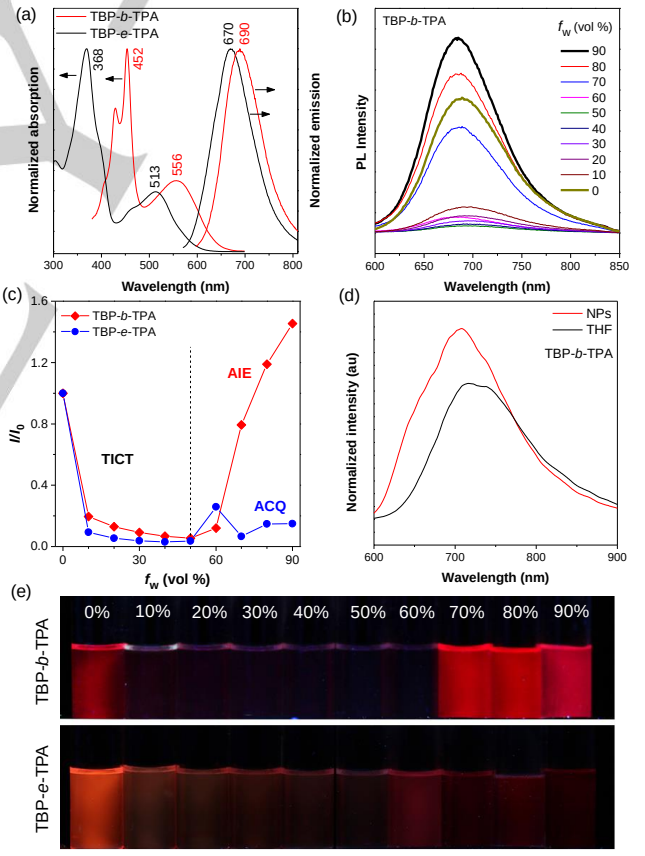


**Figure 2.** Optical properties of TBP-*b*-TPA and TBP-*e*-TPA. (a) Normalized absorption and emission profile in THF. (b) PL spectra of TBP-*b*-TPA in THF/$H_2O$ mixture with different $f_w$. (c) Variation in PL intensity ($I/I_0$) of TBP-*b*-TPA and TBP-*e*-TPA with $f_w$, where $I_0$ and $I$ were the maximal PL intensity. (d) 2PF spectra of TBP-*b*-TPA in THF and water (NPs), respectively (0.1 mg/mL). (e) Fluorescent photos of TBP-*b*-TPA and TBP-*e*-TPA at different $f_w$ (365 nm hand-held UV lamp irradiation).

10.1002/anie.202005785




To demonstrate the feasibility of the present strategy, the photophysical properties of the two molecules are investigated. As displayed in Figure 2a, TBP-*e*-TPA and TBP-*b*-TPA featured two primary absorption bands typical of donor-acceptor-donor fluorophores. The second band at lower energy (513 and 556 nm) is attributed to intramolecular charge transfer (ICT) transition to electron-deficient TBP unit from the electron-rich TPA unit.[13] To further study the ICT transition, density functional theory (DFT) calculations for two dyes were carried out (Figure S7, S8). The higher extent of spatial separation of the highest occupied and the lowest unoccupied molecular orbitals in TBP-*b*-TPA than that of TBP-*b*-TPA, demonstrating a stronger ICT character.[14] TBP-*b*-TPA had an emission maximum of 690 nm at near-infrared (NIR) region, slightly red-shifted compared to that of TBP-*e*-TPA (670 nm). The relatively small Stokes shift in TBP-*b*-TPA (134 nm) and TBP-*e*-TPA (157 nm) than the twisted NIR molecules indicated the planarization-dominated structures.[15] To verify the aggregate-state emission, PL spectra were performed to monitor the emission intensity fluctuation of the molecules in THF/$H_2O$ mixtures with various water volume fractions ($f_w$). As shown in Figure 2b and S9, two molecules displayed strong emission in THF due to the presence of a large π-conjugated planar structure. Upon enhancing $f_w$ from 0 to 50 vol%, a significant decrease in fluorescence intensity was observed, owing to dark twisted intramolecular charge transfer (TICT) state (a weakly emissive $S_1$ excited state) being formed with an increase of polarity (Figure 2c, S10, S11, Table S1).[16] Further increase of $f_w$ to 90 vol%, the AIE effect turns on the emission because the intramolecular rotation necessary for the formation of a TICT state is hindered upon molecular aggregation.[17] TBP-*b*-TPA gave a high PLQY both in solution (16.2% ± 0.4%) and crystal state (15.6 % ± 0.2%). In contrast, the PLQY of TBP-*e*-TPA decreased significantly from solution (8.9% ± 0.6%) to crystal (0.2% ± 0.1%) (Figure 2e). The distinct difference in solid-state QY suggested a significant effect of molecular packing.

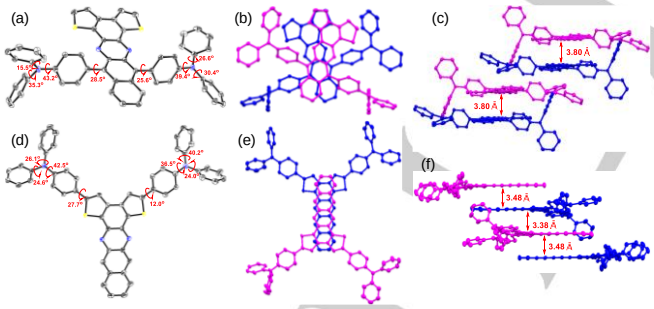


**Figure 3.** Crystal structures. (a-c) Single crystal structure (a), dimer structure (b) and molecular π-π stacking structures (c) of TBP-*b*-TPA. (d-f) Single crystal structure (d), dimer structure (e) and molecular π-π stacking structures (f) of TBP-*e*-TPA.

On the other hand, benefiting from the conjugated structure with strong push-pull dipolar characteristics of the dyes, excellent nonlinear optical properties such as a two-photon excitation spectrum could be anticipated.[12b, 18] Compared to one-photo excitation imaging, it was reasoned that two-photo excitation showed salient advantages of deep penetration depth and high resolution owing to the excitation wavelength's redshift towards the biological window (700-1100 nm) and the two-photo excitation's intrinsic confocal nature. The two-photon absorption cross section ($\delta_{2PA}$) of TBP-*b*-TPA was calculated to be 608 ± 9 GM at 880 nm (700-1000 nm, NIR-I region) and 207 ± 7 GM at 1040 nm (1000-1700 nm, NIR-II region) (Figure S12).[18b, 19] Considering the acceptable $\delta_{2PA}$ and the reduced photon scattering and autofluorescence in NIR-II region, the 1040 nm-excited two-photon fluorescence (2PF) property of TBP-*b*-TPA in aggregate state was then explored. As shown in Figure 2d and Figure S13, TBP-*b*-TPA possessed boosted 2PF signal in nanoparticle state than that of in THF. These data strongly indicated the tuning of molecular packing to attain excellent 2PA property at the biological transparency window.[20] The distinct emission properties (AIE vs ACQ) of the regioisomers in aggregate served as motivation to elucidate their molecular arrangement in the crystals. Crystallographic structures of TBP-*b*-TPA and TBP-*e*-TPA were displayed in Figure 3a, d, Table S2-S5.[21] As expected, the TBP core is planar for the two molecules. TBP-*b*-TPA adopted a "+" shape confirmation, while a "Y" shape was observed in its regioisomer (Figure 3a, 3d). The dihedral angles between TPA and TBP core in TBP-*b*-TPA were 28.5° and 25.6°, which was similar to that of TBP-*b*-TPA (27.7° and 12.0°), indicating that the distortion between TPA and TBP. As displayed in Figure 3b, the crystal packing's most attractive structural feature was that TBP-*b*-TPA molecules overlapped upon the central phenyl rings directly connected with TPA units, and one molecule was rotated relative to the other by an angle of 42°. We reasoned that such a cross packing mode was due to the steric hindrance effect of the *bay*-located TPA unit. The crystal packing diagram in TBP-*b*-TPA showed that there were nearly no π-π interactions among the discrete dimers (3.80 Å), which favored strong solid-state fluorescence (Figure 3c).[22] Whereas, TBP-*e*-TPA dimer adopted a complete face-to-face π-π interaction between the central TBP units in a tail-to-tail way, because of the driving force from the *end*-located TPA (Figure 3e). Moreover, a long-range cofacial packing mode (3.48 Å and 3.38 Å) was observed, where the excited-state energy might non-radiatively be consumed and thus showed quenched fluorescence in crystals (Figure 3f). Thereof, through tuning molecular packing from a long-range cofacial mode to a discrete cross packing by regioisomerization, highly bright solid-state fluorescence was realized.

Based on the excellent photophysical properties of TBP-*b*-TPA, we then investigated its potential for bioimaging. To endow colloidal stability and desirable blood circulation time, TBP-*b*-TPA was formulated into nanoparticles (TBP-*b*-TPA NPs) using amphiphilic block copolymer DSPE-PEG via a typical nanoprecipitation method (Figure 4a).[23] Transmission electron microscopy (TEM) and dynamic light scattering (DLS) results indicated the resultant NPs with a diameter of ~99 nm (Figure S14). Moreover, TBP-*b*-TPA NPs displayed good biocompatibility and photostability (Figure S15, S16). Then we evaluated the imaging ability of TBP-*b*-TPA NPs for Hela cells using confocal laser scanning microscopy (CLSM). As shown in Figure 4b, the appearance of a reticulum-like red-fluorescence image of HeLa cells indicated that the dyes might localize at mitochondria, which verified by a colocalization experiment with a commercial mitochondria-specific agent, MitoTracker Green (MTG). The regions stained with TBP-*b*-TPA NPs overlapped well with that of MTG, indicating a high specificity to mitochondria with a Pearson coefficient of ~0.903. We then evaluate whether TBP-*b*-TPA is suitable for two-photon imaging with NIR-I emission and NIR-II

10.1002/anie.202005785




excitation. The fluorescence signals (collected from 700-800 nm) from two-photon imaging irradiated by a NIR-II pulsed laser at 1040 nm displayed almost identical distribution with that of one-photon imaging. It was widely reported that 2PF microscopy (2PFM) holds the merits of deeper penetration depth, lower photodamage, and better 3D resolution compared to one-photon microscopy.[24] Thus, TBP-*b*-TPA NPs showed great potential for two-photon imaging in live tissues.

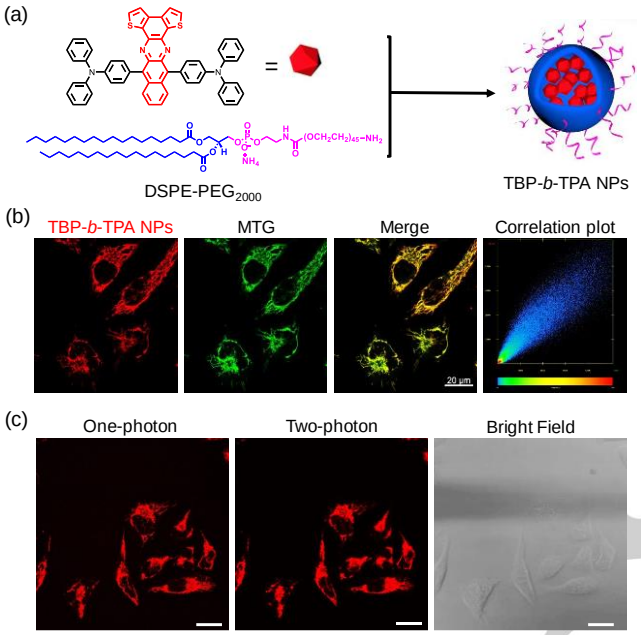


**Figure 4.** (a) Schematic illustration of the preparation of TBP-*b*-TPA NPs. (b) CLSM images of HeLa cells incubated with TBP-*b*-TPA NPs ($\lambda_{ex}$ = 560 nm, $\lambda_{em}$ = 600~700 nm) and MTG ($\lambda_{ex}$ = 488 nm, $\lambda_{em}$ = 500-525 nm). (c) One-photon ($\lambda_{ex}$ = 560 nm, $\lambda_{em}$ = 700-800 nm) and Two-photon ($\lambda_{ex}$ = 1040 nm, $\lambda_{em}$ = 700-800 nm) fluorescent microscopic images of Hela cells incubated with TBP-*b*-TPA NPs. Scale bar = 20 μm.

To examine the feasibility of the AIE NPs for visualizing the cortical vascular architecture, we further carried out in vivo 2PFM imaging to construct 3D vasculature information. The 2PFM scanned the mouse brain after intravenous injection of the TBP-*b*-TPA NPs. The brain vasculature at different depths could be detected with high clarity (Figure 5), and the vasculature could also be observed even at 700 μm. The apparent diameters of the vessel were ~1.55 μm and 1.80 μm at a depth of 400 and 600 μm, respectively, which were higher than some reported ones irradiated with 1040 nm.[25] After reconstructing the 3D image of the cortical vasculature from bottom to top, we can distinctly visualize the major blood vessels, tiny capillaries, and junctions at the same time. These excellent results revealed that TBP-*b*-TPA NPs hold considerable potentials for 2PF imaging with deep penetration and high-resolution.

In summary, unlike traditional ACQ-to-AIE transformation molecular design philosophy which relies on twisted conformation for suppressing intermolecular interactions, for the first time, through tuning molecular packing mode by regioisomerization, a

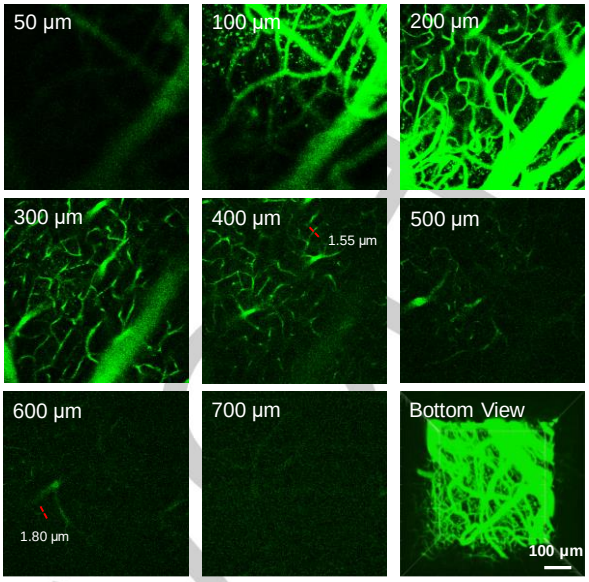


**Figure 5.** In vivo 2PFM imaging of TBP-*b*-TPA NPs stained cortical vasculature at various depths as indicated and 3D reconstruction of the vasculature from top to 700 μm depth. Excitation wavelength: 1040 nm (50 MHz). Dichroic mirror for two-photon fluorescence collection: 800 nm short-pass.

new strategy for highly bright solid-state fluorescence emission has been realized. The ACQ-dominated TBP-*e*-TPA adopts a long-range molecular packing mode, while the AIE-active TBP-*b*-TPA shows a discrete cross packing mode. This molecular design strategy provides new insight to convert traditional ACQ luminogens into AIE ones without destroying the high π-conjugation structure. Meanwhile, TBP-*b*-TPA exhibited a sizeable two-photon absorption cross-section of up to 207 ± 7 GM under the 1040 nm excitation. In vivo 2PF brain imaging displayed deep penetration and high-resolution with NIR-I emission and NIR-II excitation. The present work provides a novel strategy to develop solid-state organic luminogens for biomedical imaging and other applications like organic light-emitting diodes and luminescent devices.

## Acknowledgements

This work was financially supported by the National Natural Science Foundation of China (51903052), Shanghai Pujiang Project (19PJ1400700), Zhejiang Provincial Natural Science Foundation of China LR17F050001, the National Science Foundation of China (21788102, 21805002, 61735016 and 61975172), the Research Grants Council of Hong Kong (16305518, N-HKUST609/19, A-HKUST605/16, AoE/P-01/12 and C6009-17G), the Innovation and Technology Commission (ITC-CNERC14SC01 and ITCPD/17-9) and the Science and Technology Plan of Shenzhen (JCYJ20180507183832744 and JCYJ20180306180231853). We gratitude the X-ray single crystal structural analyses by Herman H. Y. Sung and Ian D. Williams.

**Keywords:** aggregation-induced emission • cross packing • regioisomerization • ACQ-to-AIE transformation • two-photon imaging

[1] a) S. P. Anthony, *ChemPlusChem* **2012**, *77*, 518-531; b) R. Davis, N. S. Saleesh Kumar, S. Abraham, C. H. Suresh, N. P. Rath, N. Tamaoki, S. Das, *J. Phys. Chem. C* **2008**, *112*, 2137-2146.

[2] J. Mei, N. L. C. Leung, R. T. K. Kwok, J. W. Y. Lam, B. Z. Tang, *Chem. Rev.* **2015**, *115*, 11718-11940.

[3] J. Luo, Z. Xie, J. W. Y. Lam, L. Cheng, H. Chen, C. Qiu, H. S. Kwok, X. Zhan, Y. Liu, D. Zhu, B. Z. Tang, *Chem. Commun.* **2001**, 1740-1741.

[4] a) S. Liu, Y. Li, H. Zhang, Z. Zhao, X. Lu, J. W. Y. Lam, B. Z. Tang, *ACS Materials Letters* **2019**, *1*, 425-431; b) H. Zhang, Z. Zhao, P. R. McGonigal, R. Ye, S. Liu, J. W. Y. Lam, R. T. K. Kwok, W. Z. Yuan, J. Xie, A. L. Rogach, B. Z. Tang, *Mater. Today* **2020**, *32*, 275-292; c) Y. Li, S. Liu, T. Han, H. Zhang, C. Chuah, R. T. K. Kwok, J. W. Y. Lam, B. Z. Tang, *Mater. Chem. Front.* **2019**, *3*, 2207-2220; d) J. Qian, B. Z. Tang, *Chem* **2017**, *3*, 56-91; e) D. Ding, K. Li, B. Liu, B. Z. Tang, *Acc. Chem. Res.* **2013**, *46*, 2441-2453; f) J. Yang, Z. Ren, B. Chen, M. Fang, Z. Zhao, B. Z. Tang, Q. Peng, Z. Li, *J. Mater. Chem. C* **2017**, *5*, 9242-9246.

[5] Y. Li, Z. Cai, S. Liu, H. Zhang, S. T. H. Wong, J. W. Y. Lam, R. T. K. Kwok, J. Qian, B. Z. Tang, *Nat. Commun.* **2020**, *11*, 1255.

[6] S. Liu, C. Chen, Y. Li, H. Zhang, J. Liu, R. Wang, S. T. H. Wong, J. W. Y. Lam, D. Ding, B. Z. Tang, *Adv. Funct. Mater.* **2020**, *30*, 1908125.

[7] a) L. Zong, Y. Xie, C. Wang, J.-R. Li, Q. Li, Z. Li, *Chem. Commun.* **2016**, *52*, 11496-11499; b) Z. Zhao, P. Lu, J. W. Y. Lam, Z. Wang, C. Y. K. Chan, H. H. Y. Sung, I. D. Williams, Y. Ma, B. Z. Tang, *Chem. Sci.* **2011**, *2*, 672-675; c) N. Xie, Y. Liu, R. Hu, N. L. C. Leung, M. Arseneault, B. Z. Tang, *Isr. J. Chem.* **2014**, *54*, 958-966.

[8] Q. Zhao, S. Zhang, Y. Liu, J. Mei, S. Chen, P. Lu, A. Qin, Y. Ma, J. Z. Sun, B. Z. Tang, *J. Mater. Chem.* **2012**, *22*, 7387-7394.

[9] H.-Q. Peng, X. Zheng, T. Han, R. T. K. Kwok, J. W. Y. Lam, X. Huang, B. Z. Tang, *J. Am. Chem. Soc.* **2017**, *139*, 10150-10156.

[10] L. Ji, Y. Zhao, M. Tao, H. Wang, D. Niu, G. Ouyang, A. Xia, M. Liu, *ACS Nano* **2020**, *14*, 2373-2384.

[11] S. Pratihar, A. Bhattacharyya, E. Prasad, *J. Photochem. Photobiol. A: Chem.* **2020**, 112458.

[12] a) A. Shao, Y. Xie, S. Zhu, Z. Guo, S. Zhu, J. Guo, P. Shi, T. D. James, H. Tian, W.-H. Zhu, *Angew. Chem. Int. Ed.* **2015**, *54*, 7275-7280; b) Z. Zheng, T. Zhang, H. Liu, Y. Chen, R. T. K. Kwok, C. Ma, P. Zhang, H. H. Y. Sung, I. D. Williams, J. W. Y. Lam, K. S. Wong, B. Z. Tang, *ACS Nano* **2018**, *12*, 8145-8159; c) H. Lu, Y. Zheng, X. Zhao, L. Wang, S. Ma, X. Han, B. Xu, W. Tian, H. Gao, *Angew. Chem. Int. Ed.* **2016**, *55*, 155-159; d) M. Shimizu, R. Kaki, Y. Takeda, T. Hiyama, N. Nagai, H. Yamagishi, H. Furutani, *Angew. Chem. Int. Ed.* **2012**, *51*, 4095-4099; e) Q. Li, Z. Li, *Acc. Chem. Res.* **2020**, 53, 4, 962-973; f) Q. Li, Z. Li, *Adv. Sci.* **2017**, *4*, 1600484-1600484; g) Q. Li, Z. Li, *Sci China Mater* ***2020****, 63, 177-184;* h) H. Wu, W. Chi, G. Baryshnikov, B. Wu, Y. Gong, D. Zheng, X. Li, Y. Zhao, X. Liu, H. Ågren, L. Zhu, *Angew. Chem. Int. Ed.* **2019**, *58*, 4328-4333.

[13] S. Liu, H. Zhang, Y. Li, J. Liu, L. Du, M. Chen, R. T. K. Kwok, J. W. Y. Lam, D. L. Phillips, B. Z. Tang, *Angew. Chem. Int. Ed.* **2018**, *57*, 15189-15193.

[14] H. Tanaka, K. Shizu, H. Nakanotani, C. Adachi, *Chem. Mater.* **2013**, *25*, 3766-3771.

[15] a) J. Qi, C. Sun, D. Li, H. Zhang, W. Yu, A. Zebibula, J. W. Y. Lam, W. Xi, L. Zhu, F. Cai, P. Wei, C. Zhu, R. T. K. Kwok, L. L. Streich, R. Prevedel, J. Qian, B. Z. Tang, *ACS Nano* **2018**, *12*, 7936-7945; b) Z. H. Sheng, B. Guo, D. H. Hu, S. D. Xu, W. B. Wu, W. H. Liew, K. Yao, J. Y. Jiang, C. B. Liu, H. R. Zheng, B. Liu, *Adv. Mater.* **2018**, *30*.

[16] a) S. Liu, X. Zhou, H. Zhang, H. Ou, J. W. Y. Lam, Y. Liu, L. Shi, D. Ding, B. Z. Tang, *J. Am. Chem. Soc.* **2019**, *141*, 5359-5368; b) R. Hu, E. Lager, A. Aguilar-Aguilar, J. Liu, J. W. Y. Lam, H. H. Y. Sung, I. D. Williams, Y. Zhong, K. S. Wong, E. Peña-Cabrera, B. Z. Tang, *J. Phys. Chem. C* **2009**, *113*, 15845-15853; c) M. Borelli, G. Iasilli, P. Minei, A. Pucci, *Molecules* **2017**, *22*, 1306; d) D. Liese, G. Haberhauer, *Isr. J. Chem.* **2018**, *58*, 813-826.

[17] S. Liu, Y. Cheng, H. Zhang, Z. Qiu, R. T. Kwok, J. W. Lam, B. Z. Tang, *Angew. Chem. Int. Ed.* **2018**, *57*, 6274-6278.

[18] a) M. Albota, D. Beljonne, J.-L. Brédas, J. E. Ehrlich, J.-Y. Fu, A. A. Heikal, S. E. Hess, T. Kogej, M. D. Levin, S. R. Marder, *Science* **1998**, *281*, 1653-1656; b) G. Niu, X. Zheng, Z. Zhao, H. Zhang, J. Wang, X. He, Y. Chen, X. Shi, C. Ma, R. T. K. Kwok, J. W. Y. Lam, H. H. Y. Sung, I. D. Williams, K. S. Wong, P. Wang, B. Z. Tang, *J. Am. Chem. Soc.* **2019**, *141*, 15111-15120; c) M. Pawlicki, H. A. Collins, R. G. Denning, H. L. Anderson, *Angew. Chem. Int. Ed.* **2009**, *48*, 3244-3266.

[19] N. S. Makarov, M. Drobizhev, A. Rebane, *Opt. Express* **2008**, *16*, 4029-4047.

[20] a) M. Jiang, X. Gu, J. W. Y. Lam, Y. Zhang, R. T. K. Kwok, K. S. Wong, B. Z. Tang, *Chem. Sci.* **2017**, *8*, 5440-5446; b) M. Pawlicki, H. A. Collins, R. G. Denning, H. L. Anderson, *Angew. Chem. Int. Ed.* **2009**, *48*, 3244-3266; c) J. Massin, A. Charaf-Eddin, F. Appaix, Y. Bretonnière, D. Jacquemin, B. van der Sanden, C. Monnereau, C. Andraud, *Chem. Sci.* **2013**, *4*, 2833-2843; d) S. Sumalekshmy, C. J. Fahrni, *Chem. Mater.* **2011**, *23*, 483-500.

[21] X. Lu, S. Lee, Y. Hong, H. Phan, T. Y. Gopalakrishna, T. S. Herng, T. Tanaka, M. E. Sandoval-Salinas, W. Zeng, J. Ding, D. Casanova, A. Osuka, D. Kim, J. Wu, *J. Am. Chem. Soc.* **2017**, *139*, 13173-13183.

[22] Z. Xie, B. Yang, F. Li, G. Cheng, L. Liu, G. Yang, H. Xu, L. Ye, M. Hanif, S. Liu, D. Ma, Y. Ma, *J. Am. Chem. Soc.* **2005**, *127*, 14152-14153.

[23] H.-B. Cheng, Y. Li, B. Z. Tang, J. Yoon, *Chem. Soc. Rev.* **2020**, *49*, 21-31.

[24] M. Jiang, X. Gu, J. W. Y. Lam, Y. Zhang, R. T. K. Kwok, K. S. Wong, B. Z. Tang, *Chem. Sci.* **2017**, *8*, 5440-5446.

[25] a) N. Alifu, X. Dong, D. Li, X. Sun, A. Zebibula, D. Zhang, G. Zhang, J. Qian, *Mater. Chem. Front.* **2017**, *1*, 1746-1753; b) W. Qin, N. Alifu, Y. Cai, J. W. Y. Lam, X. He, H. Su, P. Zhang, J. Qian, B. Z. Tang, *Chem. Commun.* **2019**, *55*, 5615-5618.

10.1002/anie.202005785

WILEY-VCH

COMMUNICATION

## Entry for the Table of Contents

Insert graphic for Table of Contents here.

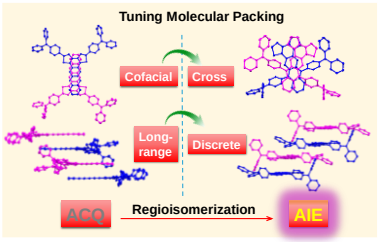


**Solid-state fluorescence:** traditional methods of designing bright solid-state fluorescent materials rely on suppressing the π-π interactions. This work proposed a strategy of tuning molecular packing mode by regioisomerization. Changing the molecular packing from long-range coficial mode to a discrete cross packing one can realize ACQ-to-AIE transformation, achieving highly bright solid-state materials.

Institute and/or researcher Twitter usernames: @BenZhongTANG1